Biopolymers
March 2009, Volume 91, Issue 3, Pages 207 - 220
http://dx.doi.org/10.1002/bip.21119

NMR structure of *r*ALF-*Pm3*, an anti-lipopolysaccharide factor from shrimp: Model of the possible lipid A-binding site

Yinshan Yang[1], Hélène Boze[2], Patrick Chemardin[2], André Padilla[1], Guy Moulin[2], Anchalee Tassanakajon[3], Martine Pugnière[4], Françoise Roquet[4], Delphine Destoumieux-Garzón[5], Yannick Gueguen[5], Evelyne Bachère[5], André Aumelas[1, *]

[1] CNRS UMR5048; INSERM, U554; Université Montpellier 1 et 2, Centre de Biochimie Structurale, 29 rue de Navacelles, 34090 Montpellier, Cedex 9, France
[2] UMR SPO INRA, Génie Microbiologique et Enzymatique, Batiment 32, 2 Place Viala, 34060 Montpellier, Cedex 1, France
[3] Shrimp Molecular Biology and Genomics Laboratory, Department of Biochemistry, Faculty of Science, Chulalongkorn University, Bangkok 10330, Thailand
[4] Université Montpellier 1, CPBS; CNRS UMR 5236 (CPBS); Université Montpellier 2, CPBS, F-34095 Montpellier, Cedex 5, France
[5] Ifremer, CNRS, Université de Montpellier 2, UMR 5119 Ecosystèmes Lagunaires, CC 80, Place E. Bataillon, 34095 Montpellier, Cedex 5, France

*: Corresponding author : André Aumelas, email address : aumelas@cbs.cnrs.fr

Abstract:

The anti-lipopolysaccharide factor ALF-*Pm3* is a 98-residue protein identified in hemocytes from the black tiger shrimp *Penaeus monodon*. It was expressed in *Pichia pastoris* from the constitutive glyceraldehyde-3-phosphate dehydrogenase promoter as a folded and ^{15}N uniformly labeled *r*ALF-*Pm3* protein. Its 3D structure was established by NMR and consists of three α-helices packed against a four-stranded β-sheet. The C^{34}—C^{55} disulfide bond was shown to be essential for the structure stability. By using surface plasmon resonance, we demonstrated that *r*ALF-*Pm3* binds to LPS, lipid A and to OM®-174, a soluble analogue of lipid A. Biophysical studies of *r*ALF-*Pm3*/LPS and *r*ALF-*Pm3*/OM®-174 complexes indicated rather high molecular sized aggregates, which prevented us to experimentally determine by NMR the binding mode of these lipids to rALF-*Pm3*. However, on the basis of striking structural similarities to the FhuA/LPS complex, we designed an original model of the possible lipid A-binding site of ALF-*Pm3*. Such a binding site, located on the ALF-*Pm3* β-sheet and involving seven charged residues, is well conserved in ALF-L from *Limulus polyphemus* and in ALF-T from *Tachypleus tridentatus*. In addition, our model is in agreement with experiments showing that β-hairpin synthetic peptides corresponding to ALF-L β-sheet bind to LPS. Delineating lipid A-binding site of ALFs will help go further in the *de novo* design of new antibacterial or LPS-neutralizing drugs.

ABBREVIATIONS

3D, three-dimensional

ALF, anti-lipopolysaccharide factor;

ALF-*Pm1,2,3,4* isoforms 1,2,3,4 of the anti-lipopolysaccharide factors of *Penaeus monodon;*

ALF-L, anti-lipopolysaccharide factor of *Limulus polyphemus;*

ALF-T, anti-lipopolysaccharide factor of *Tachypleus tridentatus;*

CMC, critical micellar concentration;

DQF-COSY, 2D double-quantum filter correlation spectroscopy;

DTT, Dithiothreitol;

GAP, glyceraldehyde-3-phosphate dehydrogenase promoter

HSQC, heteronuclear single-quantum coherence;

LPS, lipopolysaccharide;

NMR, nuclear magnetic resonance;

NOE, nuclear Overhauser effect;

NOESY, 2D nuclear Overhauser effect spectroscopy;

OM®-174, the code name for the water soluble 3-3'-O-deacylated *E. coli* lipid A analogue;

rmsd, root mean square deviation;

SPR, surface plasmon resonance;

TOCSY, total correlation spectroscopy;

TPPI, time proportional phase incrementation;

KEYWORDS

anti-lipopolysaccharide factor, lipopolysaccharide, lipid A, NMR, structure, septic shock, surface plasmon resonance, ultracentrifugation.

INTRODUCTION

Anti-lipopolysaccharide factors (ALFs), originally characterized from horseshoe crabs, have been recently identified from hemocytes of different shrimp species, *Penaeus monodon (1*), *Litopenaeus setiferus, L. vannamei (2*) and *L. stylirostris* (Genbank AAY 33769)*(3*) *Fenneropenaeus chinensis (4*), *Marsupenaeus japonicus (5*), and recently from the mud crab, *Scylla paramamosain (6*). ALFs consist in a small basic single polypeptide of about 100 amino acids with two conserved cysteine residues forming a disulfide bond that constrains a β-hairpin *(7, 8*). In ALF-*Pm*3 from the shrimp *P. monodon,* positively-charged residues are clustered within the β-hairpin. Antimicrobial assays demonstrated that the recombinant *r*ALF-*Pm*3 has a broad spectrum of antifungal properties against filamentous fungi, and antibacterial activities against both Gram-positive and Gram-negative bacteria, associated with a bactericidal effect *(1*). Interestingly, *r*ALF-*Pm*3 is highly efficient against various *Vibrio* species including s shrimp pathogens. Consistently, RNA interference (RNAi) experiments targeting an ALF gene from the shrimp *L. vannamei* resulted in increased susceptibility to pathogenic *Vibrio* and *Fusarium* species *(9*). In the freshwater crayfish *Pacifastacus leniusculus*, RNAi showed that the crayfish ALF can protect against infection by the white spot syndrome virus, a virus infecting many different species of crustaceans *(4*).

The *Limulus polyphemus* ALF (ALF-L), which has a strong antibacterial effect on the growth of Gram-negative bacteria *(10*), was also demonstrated to interact with lipid A, the conserved hydrophobic region of lipopolysaccharides (LPS or endotoxin) that constitutes the bioactive core and toxic component of LPS. Immune cells from both vertebrates and invertebrates are highly sensitive to LPS, which are recognized as non-self molecules and rapidly initiate an immune response. Through its potent LPS-neutralizing effect, ALF-L was initially evidenced as a factor able to prevent the hemolymph clotting resulting from immune cell activation in the horseshoe crab *(11*). In vertebrates, LPS recognition is mediated by type-4 Toll-like receptors (TLR4) *(12-14*). Their interaction induces the release of cytokines, tumor-necrosis α-factor (TNF-α) and interleukins leading to the septic shock. Interaction between ALF and lipid A prevents from the

cascade of events responsible for the release of mediators and thus protects against the endotoxin-induced septic shock.

The ALF-L crystal structure was solved and consists of a four-stranded β-sheet and three helices giving rise to a wedge-shaped molecule *(8*). Based on this structure, a lipid A-binding region was proposed which involves the β-hairpin stabilized by the single disulfide bond. The positively-charged residues within the β-hairpin of ALF-L were supposed to interact with the negatively charged phosphate groups of lipid A. On this basis, some synthetic peptides were developed to protect from the septic shock *(15*). However, as far as we know, the binding site between ALF proteins and lipid A remains poorly studied and is still unknown. Thus, the aim of the present work was to determine the solution structure of the *r*ALF-*Pm3* and identify the lipid A-binding site from the structural study of the *r*ALF-*Pm3*/LPS complex.

In this attempt, we expressed *r*ALF-*Pm3* as an uniformly ^{15}N-labeled protein in *Pichia pastoris* from the constitutive glyceraldehyde-3-phosphate dehydrogenase (GAP) promoter. The three-dimensional (3D) solution structure of *r*ALF-*Pm3* was determined by NMR. Its interaction with LPS, with lipid A from *Escherichia coli*, and with OM®-174 was then studied by surface plasmon resonance (SPR), NMR and ultracentrifugation. OM®-174, the water soluble analogue of lipid A, was selected with the aim to improve the complex solubility. Unfortunately, the sizes of the *r*ALF-*Pm3*/LPS and of the *r*ALF-*Pm3*/ OM®-174 complexes were too large and prevent us from the experimental determination of the *r*ALF-*Pm3* lipid A-binding site. Consequently, we used a structural comparison of the ALF-*Pm3* structure with that of the FhuA/LPS complex, to propose a model of the ALF-*Pm3* lipid A binding site. We believe that the knowledge of *r*ALF-*Pm3* 3D structure would be very helpful for the design of new drugs to fight septic shock.

MATERIALS AND METHODS

Materials- Lipopolysaccharide (LPS) from *E. coli* O111:B4 and Lipid A, monophosphoryl from *E. coli* F583 (Rd mutant) were purchased from Sigma. The water soluble OM®-174 analogue was kindly provided by OM-PHARMA, Meyrin/Geneva (Switzerland) *(16*).

Sequence alignments- The ALF sequences of *Limulus polyphemus*, *Tachypleus tridentatus* and *Penaeus monodon* were aligned with the TCoffee program available on the web (http://www.ch.embnet.org/software/TCoffee.html).

Construction of the pGAP ALF-Pm3 new vector- pGAPZαB plasmid utilizes the constitutive glyceraldehyde-3-phosphate dehydrogenase (GAP) promoter of *P. pastoris* and the α-factor leader sequence of *S. cerevisiae* for product secretion. ALF-*Pm3* gene was extracted from the construction previously described *(1*) and transferred into a pGAPZαB plasmid (Invitrogen). For this, the pPIC9K plasmid containing *ALF-Pm3* was digested by XhoI and NotI restriction enzymes. The DNA fragment containing the gene of interest was isolated by agarose gel electrophoresis and then purified using a Geneclean kit (Bio 101 InC., Vista, CA, USA). The pGAPZαB plasmid was digested using XhoI and NotI before its ligation with *ALF-Pm3* using phage T4 DNA ligase. After transformation of *E. coli* XL1-Blue MRF (Stratagene, La Jolla, CA, USA), positive clones were selected by zeocin resistance. After checking the insertion of *ALF-Pm3* in pGAP with the correct orientation (*E. coli* XL1/pGAP ALF-*Pm3*), this plasmid was used as a source ALF-*Pm3* expression cassette (5'AOX α-mating factor-ALF-*Pm3*-3'AOX-TT3') in further cloning.

Transformation of P. pastoris- *P. pastoris* X33 strain (Invitrogen) was transformed with 10 µg of *Avr*II-linearized pGAP ALF-*Pm3* vector by electroporation according to manufacturer instructions. Recombinant clones were selected on RDB plates supplemented with zeocin (Invitrogen) after 5 days at 28°C.

*Production and purification of r*ALF-*Pm3*- The production of *r*ALF-*Pm3* by using the pGAP promoter of *P. pastoris* was studied in batch culture on glycerol. Three successive batches with 40 g/l glycerol were carried out as previously described *(17*). The production of the ^{15}N-labeled ALF-*Pm3* was carried out in an Applikon fermentor (600-ml culture) with 99.4% ^{15}N-labeled ammonium chloride (Eurisotope) as sole nitrogen source. Labeled $(NH_4)Cl$ was added from the very beginning (6.6 g/L) of the biomass production phase and during the growth phase at 20 and 25 h (7.69 g/L). *r*ALF-*Pm3* was produced during the growth phase and secreted into the culture medium. Then, it was further purified from cell-free supernatant (0.690 l) by ion-exchange chromatography on a Streamline SP column (i.d. 2 cm x 40 cm) as described previously *(1*). This single step purification on expanded-bed chromatography appeared to be a fast and efficient procedure since 3 mg of pure *r*ALF-*Pm3* were obtained and further characterized.

Circular Dichroism- Molecular ellipticity was measured in the far UV (180-300 nm) using a Chirascan dichrograph (Applied Photophysics). The protein was dissolved in water to a final

concentration of 0.1 mg/ml (8.10^{-6} M) at pH 6.9. Measurements were performed using a quartz cell with a 0.5 mm path-length, at a resolution of 1 nm. Five spectra were averaged. The percentages of secondary structures were calculated by using the Dichroweb program (www.cryst.bbk.ac.uk/cdweb/html/home.html).

NMR Spectroscopy- The pH values were measured at room temperature with a 3-mm electrode and are given uncorrected for the deuterium isotopic effect. ^{1}H chemical shifts were referenced with respect to sodium 4,4-dimethyl-4-silapentane-1-sulfonate (DSS) according to the IUPAC recommendations. Two samples containing *r*ALF-*Pm3* (≈1 mM) were prepared in 95:5 H_2O:D_2O and in 99.98% D_2O, respectively. The pH was adjusted to 6.9 by addition of DCl or NaOD.

NMR experiments were performed on a Bruker Avance 600 spectrometer equipped with a triple resonance cryoprobe and pulse field gradients. In all experiments, the carrier frequency was set at the water frequency. Double-quantum filtered-correlated spectroscopy (DQF-COSY) *(18*), z-filtered total-correlated spectroscopy (z-TOCSY) *(19*, *20*) and nuclear Overhauser effect spectroscopy (NOESY) *(21*) spectra were acquired in the phase-sensitive mode using the States-TPPI method *(22*). For spectra recorded in H_2O, and except for the DQF-COSY spectra (where low-power irradiation was used), the water resonance was suppressed by the WATERGATE method *(23*). The z-TOCSY spectra were obtained with a mixing time of 60 ms and NOESY spectra with mixing times of 100, 150 and 200 ms. To characterize overlapping spin systems, three sets of spectra were recorded at 22°C, 27°C, and 32°C. In addition, to observe and identify amide protons in fast exchange with water at pH 6.9, another data set was recorded at pH 5.4 where their exchange is slower.

A third sample was prepared with the ^{15}N-uniformly labeled protein (0.5 mM) to record ^{1}H-^{15}N-HSQC and 3D HSQC-NOESY experiments. Data were processed using both the XWINNMR and GIFA *(24*) programs. The full sequential assignment was achieved using the strategy described by Wüthrich *(25*).

The interaction of *r*ALF-*Pm3* with *E. coli* LPS or with OM®-174 -(the soluble analogue of lipid A)- was monitored by ^{1}H-^{15}N-HSQC. Two 0.5 ml samples of ^{15}N-labeled *r*ALF-*Pm3* at a concentration of ≈ 100 µM were used and titrated with LPS or with OM®-174. Up to 1 mg (≈200 µM) of LPS and 0.1 mg (≈200 µM) of OM®-174 were progressively added in the NMR samples. Twenty minutes after each addition, both 1D proton and ^{1}H-^{15}N-HSQC spectra were recorded. The signal intensities of the 1D spectra, the cross-peak intensities of the HSQC spectra and chemical shifts of these spectra were measured and compared with those of the initial spectra recorded in the absence of lipid. Intensities and volumes for all cross-peaks were measured with

the Cindy program *(26*). Both values showed a similar decrease as a function of the LPS resulting from the progressive precipitation of the *r*ALF-*Pm3*/LPS complex.

Structure Calculation- The intensity of NOESY cross-peaks were measured from the NOESY spectrum acquired at 32°C and at pH 6.9 with a mixing time of 100 ms, and were subsequently divided into five classes, according to their intensities. Very strong, strong, medium, weak, and very weak NOEs were then converted into 1.8–2.4, 1.8–2.8, 1.8–3.6, 1.8–4.4, and 1.8–5.0 Å distance constraints, respectively. For equivalent protons or non-stereo specifically assigned protons, pseudo-atoms were introduced. The ϕ angle restraints were derived from the $^{3}J_{NH\text{-}C\alpha H}$ coupling constants, and the $\chi 1$ angle restraints were derived from the combined analysis of the $^{3}J_{H\alpha\text{-}H\beta,\beta}$, coupling constants and intra-residues NOEs, respectively.

To calculate 3D structures, distance and dihedral angle restraints were used as input in the standard distance geometry/simulated annealing refinement and energy-minimization protocol using X-PLOR 3.8 *(27*). In the first stage of the calculation, an initial ensemble of 40 structures was generated from a template structure with randomized ϕ, ψ dihedral angles and extended side chains. In preliminary calculations, neither hydrogen bond nor the disulfide bond was used as restraint. Analyzing the obtained structures and comparing them with the NMR data permitted identification of more additional NOE restraints, which were introduced into the subsequent calculation. After a number of these refinement cycles, 1093 NOE-derived distance restraints (210 medium range and 221 long range) and 81 dihedral angles (70 ϕ, 10 χ_1, and 1 χ_2) were used as final input data. Finally, a calculation of 60 conformers including the disulfide bond was carried out, and the resulting 15 structures with a minimum of restrained violations were submitted to 5000 cycles of restrained Powell energy minimization.

Structure Analysis- The visual display and the calculation of root mean square deviation (rmsd) were performed with INSIGHT 97 (Molecular Simulation Inc., San Diego). Hydrogen bonds were considered as present if the distance between heavy atoms was less than 3.5 Å and the donor-hydrogen-acceptor angle was greater than 120°. The Ramachandran analysis was performed with PROCHECK *(28*) and the limits of the secondary structure elements and the van der Waals surfaces were determined with the STRIDE *(29*) programs. The atomic coordinates of the energy-minimized conformers of *r*ALF-*Pm3* have been deposit in the Protein Data Bank (PDB entry: 2job). Chemical shifts and NMR-constrains have been deposit in the BioMagResBank (accession number: 15622).

Finally, the 3D structure of *r*ALF-*Pm3* was compared with the ALF-L crystal structure. Not available in the PDB, this structure was kindly provided by Dr Robert Liddington and Dr Kay Diederichs *(8, 30*).

Determination of the hypothetical Lipid A-binding site of ALF-Pm3- To determine the ALF-*Pm3* lipid A-binding site, the ALF-*Pm3* solution structure was compared with the X-ray structure of the FhuA/LPS complex (PDB entry: 1qfg) *(30*). Charged residues of the 7 to 10 β-strands of the FhuA structure were found to interact with the lipid A moiety. Assuming that comparable interactions could take place between ALF-*Pm3* and Lipid A, the ALF-*Pm3* S1 to S4 strands were superimposed with the 7 to 10 β-strands of FhuA with the aim to optimize the matching of the charged side chains responsible for the Lipid A-binding.
The search was carried out visually by sliding the β-sheet structures. Among the numerous possibilities, the superimposition of the S1-S4 β-strands of ALF-*Pm3* with the 7 to 10 β-strands of FhuA, where most of positively charged and several hydrophobic residues involved in the Lipid A interaction have their counterpart in the *r*ALF-*Pm3* structure, has been selected (see Discussion).

Surface plasmon resonance study of the rALF-Pm3 interaction with LPS, Lipid A and OM®-174- All experiments were carried out on a BIACORE 3000 instrument at 25°C using HBS-N buffer [10 mM HEPES, 150 mM NaCl, pH 7.4 from Biacore AB (Uppsala, Sweden)] as a running buffer at a flow rate of 50 µl/min.
*r*ALF-*Pm3* (10 µg/ml), in 10 mM citrate buffer pH 6.2 was immobilized onto a CM5 sensor chip using the standard amine coupling method from the manufacturer (Biacore AB). The control flow cell was treated with activating reagents without the protein.
To determine their affinity for *r*ALF-*Pm3*, increasing concentrations of LPS (from 0.05 µM to 2.5 µM), of Lipid A (12.5 nM to 50 nM) and OM®-174 (12.5 nM to 50 nM) were injected onto the *r*ALF-*Pm3* (1200-2800 RU) and control flow cells. Regeneration was performed with pulses of 50 mM HCl and/or SDS 0.1%. Injections were repeated twice and sensorgrams were corrected by subtracting the control flow cell signal. The kinetic parameters were obtained from sensorgrams using BIAevaluation 3.2 software (Biacore AB) and the global fitting methods.

Ultracentrifugation and Dynamic Light Scattering experiments- Ultracentrifugation was used to measure the fraction of soluble *r*ALF-*Pm3* for various protein/lipid mixtures. Two sets of seven

*r*ALF-*Pm3* solutions of 60 µl (0.44 mg/ml), one with six LPS concentrations ranging from 0.152-2.28 mg/ml and the other with six OM®-174 concentrations ranging from 0.04-0.5 mg/ml, were prepared and incubated at room temperature for 20 min. Then, they were centrifuged on a Beckman Optima LE-80K ultracentrifuge at 100.000 g for 30 min and the protein concentration in the supernatant was monitored on a Nanodrop ND-100 UV spectrophotometer. We checked that LPS and OM®-174 had no absorbance contribution at 280 nm. Estimate of the *r*ALF-*Pm3*/LPS complex size has been obtained from Dynamic Light Scattering measurements on a Zetasizer Nano-S (Malvern Instruments Ltd) using a 70 µL sample of rALF-Pm3 at 0.45 mg/ml mixed with LPS at a concentration of 1.6 mg/ml.

RESULTS

1- Sequence alignments. A Blast search using the ALF-*Pm3* sequence as target selectively identified 26 ALF sequences from various crustacean organisms (data not shown). The most similar sequence was ALF from *Fenneropenaeus chinensis* with 87 % identity, while the most divergent sequence was the SSP12 protein of *Scylla serrata* (Mud crab) with only 25% sequence identity. Sequence alignment with the Tcoffee program (http://www.ch.embnet.org/software/TCoffee.htm) *(31*) showed significant sequence identity (about 24 %) on the ALF N-terminal half.

In contrast, the alignment of their C-terminal half of various lengths, (a 15-residue insertion and a C-terminal extension for ALF-*Pm2* and ALF-*Pm4* or a C-ter truncation for ALF-*Pm1*), showed no significant sequence identity (data not shown). Thus, the sequence alignment of ALF-*Pm3* was arbitrarily restricted to the ALF-L sequence of *Limulus polyphemus*, whose 3D structure was determined by X-ray *(8*), and ALF-T sequence of *Tachypleus tridentatus* that showed 38.2 and 34.6% identity, respectively (Figure 1). The conserved residues are spread out all along the sequence and include the two cysteines engaged in a disulfide bond. It is worth noting that most of the conserved residues in the 3 sequences are mainly hydrophobic and that they are located in similar secondary structure elements in the ALF-L X-ray structure and in the *r*ALF-*Pm3* solution structure (see Discussion).

2- Overexpression and characterization of ^{15}N-uniformly labeled rALF-Pm3.

Numerous proteins possessing disulfide bridges were successfully overexpressed in *P. pastoris* by using the methanol-inducible alcohol oxidase (AOX1) promoter *(32*). With such an expression

system, *r*ALF-*Pm3* was indeed obtained with a high yield *(1)*. Unfortunately, the protein was mainly unfolded and its two cysteines were oxidized into cysteic acid by *in situ* hydrogen peroxide (data not shown). Thus, this expression system was not suitable to yield the uniformly ^{15}N labeled *r*ALF-*Pm3*. The folded and labeled protein was obtained from another *P. pastoris* transformant, using the constitutive glyceraldehyde-3-phosphate dehydrogenase (GAP) promoter growing in glycerol medium, a system that does not lead to hydrogen peroxide release. In this case, we expected the cysteine to cysteic acid oxidation to be avoided or limited if not avoided. Indeed, the folded and ^{15}N-labeled protein was mainly obtained although mixed with 5 to 10% of the cysteic-unfolded form (data not shown). After purification, the pure protein was obtained as shown by CD, ^{1}H NMR (See supplementary material) and ^{1}H-^{15}N HSQC spectra (Figure 2).

3 - Solution structure of rALF-Pm3. The CD spectrum shows α-helical and β-strand contents of 23-28% and 23-27%, respectively, suggesting that the *r*ALF-*Pm3* 3D structure is well defined in solution. This is also supported by the spread-out of amide, aromatic and methyl resonances in the ^{1}H-NMR spectrum (See supplementary material).

The assignment of ^{1}H and ^{15}N resonances was obtained from the analysis of 2D TOCSY, 2D NOESY and 3D HSQC-NOESY spectra (see Materials and Methods) by using the strategy described by Wüthrich *(25)*. All the ^{1}H and ^{15}N resonances of the backbone and 98% of the side chains ^{1}H resonances were assigned (Figure 2). The summary of NOEs for *r*ALF-*Pm3* shows three clusters of dNN(i,i+1), dαβ(i+3) and dαN(i+4) NOEs, indicative of three helices (See supplementary material). The five N-terminal residues have no NOE and are not defined in the structure.

The structure is defined by an average of almost 11 NOEs per residue. A stereo-view of 10 ALF-*Pm3* conformers is displayed in Figure 3. For the well-defined region spanning residues E^{8} to S^{101}, the pairwise average rmsd is 0.91 ± 0.29 Å for the backbone atoms (Table 1). The Ramachandran plot (except for the glycine and proline residues) of the ten conformers indicated 83.5 and 16.0 % of the residues located in the most favored and the additional allowed regions, respectively. The structure consists of three helices (H1 to H3 spanning residues W^{7}-L^{21}, Q^{70}-K^{88} and Q^{93}-S^{101}, respectively), four β-strands (S1 to S4 spanning residues K^{26}-L^{29}, H^{32}-K^{43}, Q^{46}-W^{54} and R^{62}-T^{67}, respectively) and six β-turns, of which five are of type IV (R^{23}-K^{26}, E^{28}-G^{31}, K^{43}-Q^{46}, C^{55}-W^{58} and P^{56}-T^{59}) and one of type I' (L^{29}-H^{32}).

In the compact hydrophobic core several close distances between side-chains and aromatic rings give rise to several peculiar chemical shifts, which are briefly reported below. The amide signal

of L^{30} (5.23 ppm) is close in space to W^{99} and several alpha proton resonances are particularly upfield shifted: Q^{70} (3.03 ppm) and L^{30} (3.17 ppm) are close to Y^{49} and W^{99}, respectively. The K^{17} gamma protons (1.20 and 0.03 ppm) and K^{35} beta protons (0.64 and –0.38 ppm) displayed also unusual and nonequivalent chemical shifts due to their proximity with W^{99} and W^{54} rings, respectively (See supplementary material). Finally, the HD2 resonance of H^{32} was found particularly upfield shifted (5.77 ppm) by the W^{58} ring.

4- Comparison of the ALF-Pm3 solution structure with the X-ray structure of ALF-L. The ALF-*Pm3* structure was compared with that of ALF-L established by X-ray in 1993 *(8*). First of all, the two structures share the same α–β–β–β–β–α–α fold with secondary structure elements of comparable lengths and a similar disulfide bond (Figures 1 and 3). In these two structures, the N- and the two C-terminal helices pack against the four-stranded antiparallel β-sheet (Figure 3). Among the four strands, the S1 strand is the shortest one. The S2 and S3 strands are the longest, arranged in a β-hairpin and tightly linked together by the C^{34}-C^{55} disulfide bond and 9 hydrogen bonds in *r*ALF-*Pm3* and by the C^{31}-C^{52} disulfide bond and 10 hydrogen bonds in ALF-L.

Significant differences between the crystal structure of ALF-L and the NMR structure of ALF-*Pm3* reported here involve H1, which shifts along its main axis by about 2 Å and the S1 strand. As a result, the superimposition of backbone atoms of ALF-*Pm3* (stretch 6-102) and ALF-L (stretch 3-99) gives a 2.34 Å rmsd. Without the H1 helix, the rmsd value drops to 1.45 Å. To better identify local differences between the two structures, a superimposition using a 5 residue-sliding window was used to calculate an rmsd value as a function of the sequence number (Figure 4). Such a comparison highlights significant differences for the 18-30 and 40-50 sequences. As already indicated, the structure conservation is lower for the H1 helix and the S1 strand than in the remainder part of the structures (Figures 1 and 4). Without loops, an optimized superimposition, including S2, S3, S4, H2 and H3 fragments (50 residues) gives a rmsd of 0.95 Å pointing out to a remarkable conservation of the protein global fold.

Only few conserved residues belong to H1 and S1 stretches (Figures 1 and 4 and see below). Among them, W^{22} (ALF-*Pm3* numbering) adopts a quite different χ1 value (169°) when compared to W^{19} in ALF-L (-55°). In both structures this conserved tryptophane residue stacks against a phenylalanine ring (F^{36} in ALF-*Pm3*, and F^{24} in ALF-L) but is partially solvent exposed in the ALF-*Pm3* structure whereas it is buried in the ALF-L structure. We checked that such a difference does not result from the crystal packing for the ALF-L X-ray structure (data not shown).

5 - Interaction of rALF-Pm3 with Lipid A derivatives.

5-1 SPR. Using Biacore technology, LPS, lipid A and OM®-174 were shown to bind to the *r*ALF-*Pm3* protein covalently immobilized on CM5 sensorchip (Figure 5). The resulting sensorgrams were globally fitted for different lipid concentrations with the BIAevaluation 3.2 software to determine rates and equilibrium dissociation constants.

Association rate constants are faster for lipid A (k_a = 1.6 10^5 $M^{-1}s^{-1}$) than for OM®-174 (k_a = 3.7 10^4 $M^{-1}s^{-1}$) and LPS (k_a = 3.4 10^3 $M^{-1}s^{-1}$). While in the case of OM®-174 a dissociation rate (k_d = 2.4 10^{-4} s^{-1}) can be measured, leading to a K_D of 6.6 10^{-9} M, this was not the case of LPS and lipid A. As shown in Figure 5, we could not achieved dissociation of the *r*ALF-*Pm3/*LPS or lipid A complexes. According to instrumental limits we estimated these k_d values to be largely smaller than 5.0 10^{-6} s^{-1}. We just report here upper limits of K_D for lipid A (K_D < 3 10^{-11} M) and for LPS (K_D < 1.4 10^{-9} M).

5-2 NMR. With the aim to identify residues involved in the interaction with lipids, we recorded ^{1}H-^{15}N HSQC experiments of ALF-*Pm3* in presence of LPS, lipid A, and OM®-174. The first set of HSQC experiments was recorded in presence of lipid A starting with concentration of 10^{-5} M and up to 10^{-4} M. In these conditions, no change in the HSQC spectrum of the protein was observed, indicating that lipid A was not able to interact with *r*ALF-*Pm3*, probably due to its insolubility (data not shown).

In contrast, the addition of LPS (Figure 6) or OM®-174 (data not shown), which have higher solubility in water, progressively induced intensity decrease of the HSQC cross-peaks for all residues of the protein as shown for the *r*ALF-*Pm3*/LPS titration. According to the range of K_D values determined by SPR (10^{-9} M) we expected a slow exchange in the NMR time scale: (i.e.) intensity decrease of the free protein signals with a concomitant increase of new signals for the protein-lipid complex. Obviously, we do not observe new cross-peaks during the titration (Figure 6) and indeed, when excess of LPS or OM®-174 was added, the HSQC spectrum of the protein was no longer observed. Therefore, we suspected that the LPS or OM®-174/*r*ALF-*Pm3* complexes were too large to be observed by standard NMR techniques.

5-3 Ultracentrifugation. We needed to better characterize molecular species present in the protein/lipid complexes. The *r*ALF-*Pm3* complexes with lipids were centrifuged and the *r*ALF-*Pm3* concentration was monitored by UV spectroscopy. Results clearly showed the decrease of the protein concentration in the supernatant as a function of the LPS concentration. Moreover, these data indicate a molar ratio of 1 *r*ALF-*Pm3* for 3 LPS molecules (Figure 7). Concerning the

OM®-174 lipid, the protein/lipid molar ratio is about 1 to 15-20 (data not shown). The size of particles has been measured by DLS for the *r*ALF-*Pm3*/LPS complex. The major component (> 90%) was observed with an averaged particle diameter of 31 nm. Such a large particle size suggests a micellar structure of the *r*ALF-*Pm3*/LPS complex, which is therefore not observable in the HSQC titration.

6 - Comparison of the rALF-Pm3 structure with the X-ray structure of the FhuA/LPS complex. Hypothesis for the rALF-Pm3 lipid A-binding site. Since the ALF-*Pm3*/lipid A derivatives binding site could not be experimentally determined by NMR, we developed an original model based on a structural comparison with the X-ray structure of the FhuA/LPS complex *(30, 33*). FhuA is the receptor for ferrichrome-iron found at the *E. coli* surface that mediates the active transport of siderophores including ferrichrome into the bacteria *(34*). Its 3D structure mainly consists of a β-barrel of 22 antiparallel transmembrane β-strands. LPS is spread out on its external surface -5 out of the 6 acyl chains of lipid A are well identified - burying an area of 1800 $Å^2$. Although the FhuA protein is functionally and structurally unrelated with ALF proteins, the structure of this complex affords a well-defined network of interactions between a protein and the lipid A, which we considered as representative of the lipid A-binding site. Eight amino acids interacting with the lipid A and Kdo (3-deoxy-D-*manno*-oct-2-ulopyranosonic acid) and Hep (L-*glycero*-D-*manno*-heptopyranose) sugars of the inner core were accurately identified *(30, 33*) (Table 2). They belong to the FhuA β7- to β11-strands. Most of these positively charged amino acids are responsible for hydrogen bonds and electrostatic interactions with negatively charged or polar groups of lipid A. In addition, one negatively charged amino acids (E^{304}) hydrogen bonds with one phosphate group of lipid A. On the other hand, the 5 well-defined acyl chains of lipid A are involved in a network of hydrophobic interactions with hydrophobic amino acids of the protein allocated in two concentric clusters (F^{235}, V^{282}, F^{302}, F^{355}, F^{380} for the internal one and P^{217}, F^{231}, L^{300}, V^{357} for the external one). Altogether, these charged and hydrophobic amino acids set up the lipid A-binding site.

We hypothesized that LPS-binding proteins share a similar lipid A-binding site. Thus, a comparable network of electrostatic interactions was proposed to occur between ALF-*Pm3* and the lipid A moiety. We therefore, compared the FhuA lipid A-binding site (7 to 11 β-strands) with the 4-stranded ALF-*Pm3* β-sheet structure with the aim to get an optimal match of positively charged and hydrophobic side chains in the two structures. The β11 strand lies outside the cluster of the positively charged side chains and thus was discarded for the comparison. Numerous

superimpositions involving the ALF-*Pm3* β-sheet with the β7 to β10 FhuA strands were visually checked. As predicted, one superimposition, which involves the β7 (306-308), β8 (351-354), β9 (380-386) and β10 (436-441) strands of FhuA and the S1 (27-29), S2 (35-38), S3 (48-54) and S4 (61-66) strands of ALF-*Pm3*, gave an optimum match of charged side chains in the two structures with an rmsd of 1.38 Å for backbone atoms of 20 residues (Figure 8). Indeed, 6 positively charged amino acids K^{306} (K^{26}), K^{351} (K^{35}), R^{382} (K^{50}/K^{39}), R^{384} (R^{52}), K^{439} (R^{52}), K^{441} (K^{50}) and one negatively charged amino acid E^{304} (E^{25}) located at the FhuA molecule surface, have their counterpart in the ALF-*Pm3* structure (Table 2). Therefore, these amino acids are proposed to belong to the lipid A-binding site responsible for the interaction with the lipid A polar part. In addition, several hydrophobic side chains of FhuA (F^{355}, F^{380}, and F^{302}) interacting with acyl chains of lipid A have their counterpart in *r*ALF-*Pm3* (P^{40}/Y^{41}, Y^{48}, and W^{22}) at the lipid-sugar interface.

A similar superimposition of the ALF-L crystal structure [S1 (24-26), S2 (32-35), S3 (45-51), S4 (58-63)] with the FhuA structure [β7 (306-308), β8 (351-354), β9 (380-386) and β10 (436-441)], gave a comparable rmsd of 1.52 Å for backbone atoms of 20 residues. H^{32}/R^{34}, K^{47}/K^{36}, K^{49} and R^{61} side chains of ALF-L have their counterpart in FhuA, K^{351}, R^{382}, R^{384} and K^{439}, respectively (Table 2). Similarly, P^{37}, Y^{46}/F^{39}/W^{44} and I^{35} hydrophobic residues correspond to F^{355}, F^{380} and F^{302} in FhuA.

DISCUSSION

1 - The ALF structures. We showed here that the shrimp ALF-*Pm3* and the horseshoe crab ALF-L *(8)*, whose sequences are 38.2% identical, also have a similar structure consisting of 3 helices and a 4-stranded β-sheet. Most of the conserved amino acids were found to be hydrophobic and belong to the hydrophobic core of their structures. These include the following strictly conserved amino acids: $W^{22/19}$, $C^{34/31}$, $P^{40/37}$, $Y^{49/46}$, $C^{55/52}$, $P^{56/53}$, $W^{58/55}$, $I^{61/58}$, $V^{82/79}$ and $A^{96/93}$ (ALF-*Pm3*/ALF-L). Several other hydrophobic amino acids also contribute to the hydrophobic core stability. Altogether, they are essential to generate a comparable and stable fold. Thus, these strictly conserved hydrophobic amino acids define a topohydrophobic network *(35)*. In addition, the C^{34}-C^{55} disulfide bridge of ALF-*Pm3* displays an identical geometry as the C^{31}-C^{52} corresponding one in the ALF-L structure. This unique disulfide bond was shown to be essential for the stability of the ALF-*Pm3* 3D structure, which was found to collapse upon the disulfide bond reduction (data not shown). Charged amino acids are also conserved, being either identical

($K^{39/36}$, $R^{44/41}$, $K^{50/47}$, $E^{33/30}$ and $H^{32/29}$) or replaced by a similarly charged residue (R^{52}/K^{49}, K^{79}/R^{76}). They are solvent exposed and mainly belong to the β-sheet surface, thus affording a comparable amphipathic character for the two structures.

2- ALF-Pm3 interacts with lipid A and its derivatives. The interaction of *r*ALF-*Pm3* with lipid A, its highly water soluble derivative OM®-174, or the *E. coli* LPS was assessed both by SPR and NMR techniques. SPR was used to evaluate the association rates and equilibrium constants for lipid concentrations ranging from 12.5 to 2500 nM. The measured values indicated that *E. coli* LPS, lipid A and OM®-174 bind to ALF-*Pm3* with high affinities (apparent KD in the 10^{-9}-10^{-11} M range). Lipid A and LPS showed the highest affinities with a very slow dissociation rate of the complex, while the fastest association was measured for lipid A. The analysis of ka and KD values indicated that the lipid A and OM®-174 complexes are the most and the less stable, respectively, whereas the LPS complex shows an intermediate stability. Such a stability order of complexes follows the hydrophobic/hydrophilic ratio of the three lipids and thus suggests the essential role of the hydrophobic interactions in their stability. Indeed, this hydrophobic/hydrophilic ratio is the largest for Lipid A and the lowest for the OM-174 derivative. Despite an evident avid binding of *r*ALF-*Pm3* for all three lipids, the apparent KD values have to be interpreted with caution. Indeed, only rough estimation of LPS and lipid A CMC are available. According to the method used for their measurement, they range from 10^{-6} M *(36*) to 10^{-7}-10^{-8} M *(37*). Consequently, in our SPR experiments where lipid concentrations range from 10^{-6} to 10^{-8} M, the state of LPS and lipid A was not clear, since they potentially can adopt for the highest and lowest concentrations, the micellar and the monomeric states, respectively. In contrast, since the CMC of OM®-174 was estimated in the 10^{-3} M range, it was assumed to be monomeric in all experiments *(16*).

Clearly, ultracentrifugation data support the formation of soluble oligomers upon the formation ALF-*Pm3*/LPS and *r*ALF-Pm3/OM®-174 complexes, which would precipitate at high lipid concentrations. Yu et al. reported for LPS a CMC of 1.6 μM with aggregates of 43 molecules *(38*). Thus, LPS was probably in its micellar state in NMR experiments (10^{-4} M). Therefore, according to ultra-centrifugation data, in NMR conditions, the *r*ALF-*Pm3*/LPS and *r*ALF-Pm3/OM®-174 complexes are probably large sized oligomers (mean diameter of 31 nm) as indicated by DLS experiments. Anyway, their very high molecular size were responsible for very short T2 relaxation time, preventing us to establish the 3D structure of these complexes (Figure 6).

3- Lipid A-binding site model. On the basis of the ALF-L structure, Hoess *et al.* suggested that the S2-S3 β-hairpin stabilized by the C^{31}-C^{52} disulfide bond was a part of the lipid A-binding site *(8)*. However, there is still no structural study supporting this hypothesis. The 3D structure of rALF-*Pm3* determined here for the first time opened the way to the mapping of the lipid A-binding site. Although experimental determination was prevented by the aggregation phenomenon described above (no ALF-*Pm3*/lipid complex structure could be determined), the rALF-*Pm3* structure allowed us to further investigate the rALF-*Pm3* lipid A-binding site.

In order to map the lipid A-binding site, we compared the ALF-*Pm3* structure with the X-ray structure of FhuA in the FhuA/LPS complex. Such a comparison revealed numerous similarities and suggested for *r*ALF-*Pm3* and FhuA a similar spreading of the lipid A-binding site on the main part of the β-sheet. This binding site would involve six positively charged side chains, able to interact with the hydrophilic and phosphate groups of the lipid A. In addition, several hydrophobic amino acids involved in the LPS interaction have their counterpart in the ALF-*Pm3* structure. In FhuA, F^{355}, F^{380} and F^{302} aromatic side chains correspond to P^{40}/Y^{41}, Y^{48} and W^{22} in ALF-*Pm3*, respectively. It is worth noting that FhuA and ALF-*Pm3* structures offer to lipid A surfaces of unequal sizes. Therefore, the comparison of their binding sites is limited to their "common" surface area. However, by their flexibility, the lipid A acyl chains may surround the ALF-*Pm3* structure instead of spreading out as in the larger 22-stranded β-barrel of FhuA. Thus, hydrophobic side chains of ALF-*Pm3*, i.e. W^{22}, V^{19}, V^{38}, P^{40}, Y^{41}, L^{42}, L^{21}, V^{47}, A^{74}, and Y^{48} may be involved in hydrophobic interactions as F^{235}, P^{217}, F^{231}, V^{282}, Y^{284}, F^{302}, F^{355}, F^{380}, L^{300} and V^{357} side chains of FhuA *(30)*. Although this lipid A-binding site could not be assessed experimentally, the residues identified display a very similar spatial arrangement and clustering of several positively charged and hydrophobic side chains in both FhuA and ALF-*Pm3*. This strongly suggests that these amino acids belong to the lipid A-binding site of ALF-*Pm3*.

Besides ALF-*Pm3*, our model nicely applies to the ALF-L structure, in which the proposed lipid A-binding site is also well conserved, and to ALF-T, which is assumed to have a comparable 3D structure (Figure 1 and Table 2). Consistently, many β-hairpin derived synthetic peptides corresponding to the S2-S3 strands of ALF-L bind to LPS *(15, 39-48)*.

Interestingly, our model is also supported by the strategy used to design a biosensor for bacterial endotoxin from the green fluorescent protein (GFP) scaffold *(49)*. LPS or lipid A were previously shown to interact with short and symmetrical amphipathic cationic sequences *(49, 50)*. Accordingly, five alternating basic (B) and hydrophobic (H) residues were introduced to β-

strands located on the surface of the GFP barrel in the vicinity of the chromophore. The resulting GFP was shown to exhibit a concentration-dependent attenuation of the fluorescence intensity upon lipid A or LPS binding. As proposed here for ALF-*Pm3*, the designed binding site belongs to the β-sheet surface where the positively charged side chains of the binding site extend out to form electrostatic interactions with phosphate groups and oxygen atoms of lipid A sugars.

Finally, the size of the ALF -*Pm3*/LPS (or lipid A analogues) complex(es) clearly indicates that several *r*ALF-*Pm3* and lipid molecules are interacting. This could be mainly explained by the burying of cluster of positively charged side chains upon the LPS or lipid A analogues interactions. Such a burying and the resulting aggregation of the complexes indirectly qualify the Lys/Arg rich area of *r*ALF-*Pm3* as the lipid A binding site.

According to our model, the lipid A (LPS)-binding site of FhuA and of the two available ALF structures appears to be highly conserved. It belongs to a β-sheet structure and mainly consists of 5 to 6 positively charged residues and several hydrophobic residues able to interact through electrostatic and hydrophobic interactions with the lipid A moiety.

The residues of ALF-L identified as belonging to the lipid A-binding site in the present study are different from the four residues previously identified by using an automatic program, which positioned the binding site in the sharpest point of the structure involving both the S2-S3 loop (R^{40}, K^{41}, K^{47}) and the end of the S4 strand (K^{64}) *(30)*. Only K^{47} is common with our proposed binding site that would involve H^{32}, K^{36}, K^{47}, K^{49}, and R^{61} side chains. Thus, the binding site we propose is shifted towards the disulfide bond with a slightly concave and larger surface area allowing more hydrogen bonds, electrostatic and hydrophobic interactions. Clearly, with a spatial proximity of several basic side chains located in proximal β-strands and perpendicular to the β-sheet surface, the ALF-*Pm3* lipid A-binding site is discontinuous. In fact, it brings together several full or partial cationic binding patterns BHBHB alternating basic (B) and hydrophobic (H) residues *(49, 50*). However, the sequential amphipathic character required is here compensated for by the well-defined 3D structure in which cationic and hydrophobic side chains are clustered and solvent-exposed giving rise to the ALF-*Pm3* amphipathic feature. Moreover, the juxtaposition of several β-strands in a well-defined 3D structure generates an extended binding interface that can explain the strong interaction with lipid A derivatives.

FhuA and *r*ALF-*Pm3* proteins differ both by their location and by their function. FhuA is the receptor for ferrichrome-iron located in the membrane that mediates the active transport of siderophores, including ferrichrome into the bacteria, whereas ALFs are soluble proteins with anti microbial activities. Our model does not aim at assigning a biological significance to the similar

lipid A-binding shared by these unrelated proteins. On the one hand, the strong binding of LPS to FhuA contributes to its anchor in the bacterial outer membrane, and on the other hand, the avid binding of ALFs to LPS makes them efficient LPS-sequestrating molecules that regulate immune cell activation and contribute to the antibacterial defense of invertebrates.

Since unrelated families of cationic peptides were also demonstrated to bind LPS, the specificity of the interaction has to be questioned. This is the case for peptides derived from the silk moth cecropin and bee melittin *(51*). Similarly, surfactin, an amphiphilic cyclic lipopeptide was shown to reversibly suppress the interaction of lipid A with LPS-binding protein *(52*). When compared with lipid A, the surfactin structure possesses both negatively charged residues (Asp, Glu equivalent to phosphate groups of lipid A) and a lipophilic area including the main part of the cycle and the fatty acid chain. Interestingly, surfactin and polymyxin B are lipopeptides that share a marked amphipathic feature. Consequently, it can be hypothesized that although less specific, comparable electrostatic and hydrophobic interactions to those proposed for the *r*ALF-*Pm3* lipid A-binding site are also involved in the surfactin-LBP or the polymyxin B-LPS complexes. Recently, a 12-residue linear peptide was designed to bind LPS *(53, 54*). This peptide contains a centrally located stretch of four positively charged residues flanked by aromatic and aliphatic residues. By using transferred NOEs, such an amphipathic peptide was shown to interact with LPS in a well-folded structure and neutralize the LPS toxicity (IC_{50} ≈10 μM) with a lower efficiency than polymyxin B (IC_{50} ≈1.23 μM), the gold standard for LPS sequestration *(55*). Alternately, some anti-LPS reagents based on alkylpolyamines *(55, 56*) were also developed.

CONCLUSION

The *r*ALF-*Pm3* protein has been overexpressed in *P. pastoris* and its 3D structure determined. It displays a fold similar to that of ALF-L consisting of 3 α-helices and a 4-stranded β-sheet giving rise to a wedge-shaped molecule. Nevertheless, significant structural differences were observed in the stretch from residue 20 to 30, leading to a global shift of the N-terminal helix H1 and of the S1 strand. As shown by SPR, *r*ALF-*Pm3* displayed a high affinity for lipid A derivatives. The size of the complex was too large preventing us from determining by NMR the *r*ALF-*Pm3* residues involved in the lipid A-binding site. However, comparison of the *r*ALF-*Pm3* and ALF-L structures with that of the FhuA/LPS complex highlighted very similar clusters of positively charged and of hydrophobic residues gathered on their β-sheet surfaces. These structural similarities lead us to conclude that ALFs and FhuA display a very similar lipid A-binding site

which extends to the whole β-sheet of ALFs. Our proposed model will be very helpful to go further in the *de novo* design of LPS-binding drugs preventing septic shock. Further structural studies will help delineate the LPS binding sites of ALF proteins with more accuracy. Selected mutations along with further structural studies of ALF proteins should experimentally confirm in a near future the proposed lipid A-binding site, and open the way for the design of new anti-LPS peptides from ALF sequences and structures.

ACKNOWLEDGEMENTS

We gratefully acknowledge Dr Robert Liddington and Dr Kay Diederichs for kindly providing us the coordinates of ALF-L not available in the PDB and OM PHARMA, Meyrin/Geneva (Switzerland) for kindly providing us with the OM®-174 water-soluble lipid A analogue. We also thank Laure Sauné for precious technical assistance and the two anonymous reviewers for their insightful remarks.

.

REFERENCES

1. Somboonwiwat, K.; Marcos, M.; Tassanakajon, A.; Klinbunga, S.; Aumelas, A.; Romestand, B.; Gueguen, Y.; Boze, H.; Moulin, G.; Bachere, E. Dev Comp Immunol 2005, 29, 841-851.
2. Gross, P. S.; Bartlett, T. C.; Browdy, C. L.; Chapman, R. W.; Warr, G. W. Dev Comp Immunol 2001, 25, 565-577.
3. de Lorgeril, J.; Gueguen, Y.; Goarant, C.; Goyard, E.; Mugnier, C.; Fievet, J.; Piquemal, D.; Bachere, E. Mol Immunol 2008, 45, 3438-3445.
4. Liu, F.; Liu, Y.; Li, F.; Dong, B.; Xiang, J. Mar Biotechnol (NY) 2005, 7, 600-608.
5. Nagoshi, H.; Inagawa, H.; Morii, K.; Harada, H.; Kohchi, C.; Nishizawa, T.; Taniguchi, Y.; Uenobe, M.; Honda, T.; Kondoh, M.; Takahashi, Y.; Soma, G. Mol Immunol 2006, 43, 2061-2069.
6. Imjongjirak, C.; Amparyup, P.; Tassanakajon, A.; Sittipraneed, S. Mol Immunol 2007, 44, 3195-3203.
7. Aketagawa, J.; Miyata, T.; Ohtsubo, S.; Nakamura, T.; Morita, T.; Hayashida, H.; Iwanaga, S.; Takao, T.; Shimonishi, Y. J Biol Chem 1986, 261, 7357-7365.
8. Hoess, A.; Watson, S.; Siber, G. R.; Liddington, R. Embo J 1993, 12, 3351-3356.
9. de la Vega, E.; O'Leary, N. A.; Shockey, J. E.; Robalino, J.; Payne, C.; Browdy, C. L.; Warr, G. W.; Gross, P. S. Mol Immunol 2008, 45, 1916-1925.
10. Morita, T.; Ohtsubo, S.; Nakamura, T.; Tanaka, S.; Iwanaga, S.; Ohashi, K.; Niwa, M. J Biochem (Tokyo) 1985, 97, 1611-1620.
11. Tanaka, S.; Nakamura, T.; Morita, T.; Iwanaga, S. Biochem Biophys Res Commun 1982, 105, 717-723.
12. Beutler, B.; Rietschel, E. T. Nat Rev Immunol 2003, 3, 169-176.
13. Chaby, R. Cell Mol Life Sci 2004, 61, 1697-1713.

14. Beutler, B. Mol Immunol 2004, 40, 845-859.
15. Dankesreiter, S.; Hoess, A.; Schneider-Mergener, J.; Wagner, H.; Miethke, T. J Immunol 2000, 164, 4804-4811.
16. Brandenburg, K.; Lindner, B.; Schromm, A.; Koch, M. H.; Bauer, J.; Merkli, A.; Zbaeren, C.; Davies, J. G.; Seydel, U. Eur J Biochem 2000, 267, 3370-3377.
17. Laborde, C.; Chemardin, P.; Bigey, F.; Combarnous, Y.; Moulin, G.; Boze, H. Yeast 2004, 21, 249-263.
18. Derome, A. E.; Williamson, M. P. J Magn Reson 1990, 88, 177-185.
19. Bax, A.; Davis, G. D. J Magn Reson 1985, 65, 355-360.
20. Rance, M. J Magn Reson 1987, 74, 557-564.
21. Macura, S.; Huang, Y.; Sutter, D.; Ernst, R. R. J Magn Reson 1981, 43, 259-281.
22. Marion, D.; Ikura, M.; Tschudin, R.; Bax, A. J Magn Reson 1989, 85, 393-399.
23. Piotto, M.; Saudek, V.; Sklenar, V. J Biomol NMR 1992, 2, 661-665.
24. Pons, J. L.; Malliavin, T. E.; Delsuc, M. A. J Biolmol NMR 1996, 8, 445-452.
25. Wüthrich, K. (1986) *NMR of Proteins and Nucleic Acids*, John Wiley & sons, New York.
26. Ponchon, L.; Dumas, C.; Fesquet, D.; Padilla, A. J Biomol NMR 2004, 28, 299-300.
27. Rice, L. M.; Brunger, A. T. Proteins 1994, 19, 277-290.
28. Laskowski, R. A.; Rullmannn, J. A.; MacArthur, M. W.; Kaptein, R.; Thornton, J. M. J Biomol NMR 1996, 8, 477-486.
29. Frishman, D.; Argos, P. Proteins 1995, 23, 566-579.
30. Ferguson, A. D.; Welte, W.; Hofmann, E.; Lindner, B.; Holst, O.; Coulton, J. W.; Diederichs, K. Structure 2000, 8, 585-592.
31. Notredame, C.; Higgins, D. G.; Heringa, J. J Mol Biol 2000, 302, 205-217.
32. Klein, C.; de Lamotte-Guery, F.; Gautier, F.; Moulin, G.; Boze, H.; Joudrier, P.; Gautier, M. F. Protein Expr Purif 1998, 13, 73-82.
33. Ferguson, A. D.; Hofmann, E.; Coulton, J. W.; Diederichs, K.; Welte, W. Science 1998, 282, 2215-2220.
34. Moeck, G. S.; Coulton, J. W. Mol Microbiol 1998, 28, 675-681.
35. Colloc'h, N.; Poupon, A.; Mornon, J. P. Proteins 2000, 39, 142-154.
36. Aurell, C. A.; Wistrom, A. O. Biochem Biophys Res Commun 1998, 253, 119-123.
37. Brandenburg, K.; Andra, J.; Muller, M.; Koch, M. H.; Garidel, P. Carbohydr Res 2003, 338, 2477-2489.
38. Yu, L.; Tan, M.; Ho, B.; Ding, J. L.; Wohland, T. Anal Chim Acta 2006, 556, 216-225.
39. Ried, C.; Wahl, C.; Miethke, T.; Wellnhofer, G.; Landgraf, C.; Schneider-Mergener, J.; Hoess, A. J Biol Chem 1996, 271, 28120-28127.
40. Weiss, C. A., 3rd; Wasiluk, K. R.; Kellogg, T. A.; Dunn, D. L. Surgery 2000, 128, 339-344.
41. Vallespi, M. G.; Alvarez-Obregon, J. C.; Rodriguez-Alonso, I.; Montero, T.; Garay, H.; Reyes, O.; Arana, M. J. Int Immunopharmacol 2003, 3, 247-256.
42. Pristovsek, P.; Kidric, J. Mini Rev Med Chem 2001, 1, 409-416.
43. Arana Mde, J.; Vallespi, M. G.; Chinea, G.; Vallespi, G. V.; Rodriguez-Alonso, I.; Garay, H. E.; Buurman, W. A.; Reyes, O. J Endotoxin Res 2003, 9, 281-291.
44. Andra, J.; Lamata, M.; Martinez de Tejada, G.; Bartels, R.; Koch, M. H.; Brandenburg, K. Biochem Pharmacol 2004, 68, 1297-1307.
45. Pristovsek, P.; Kidric, J. Curr Top Med Chem 2004, 4, 1185-1201.
46. Pristovsek, P.; Simcic, S.; Wraber, B.; Urleb, U. J Med Chem 2005, 48, 7911-7914.
47. Ren, J. D.; Gu, J. S.; Gao, H. F.; Xia, P. Y.; Xiao, G. X. Int Immunopharmacol 2008, 8, 775-781.
48. Mora, P.; De La Paz, M. L.; Perez-Paya, E. J Pept Sci 2008.
49. Goh, Y. Y.; Ho, B.; Ding, J. L. Appl Environ Microbiol 2002, 68, 6343-6352.
50. Frecer, V.; Ho, B.; Ding, J. L. Eur J Biochem 2000, 267, 837-852.

51. Gough, M.; Hancock, R. E.; Kelly, N. M. Infect Immun 1996, 64, 4922-4927.
52. Takahashi, T.; Ohno, O.; Ikeda, Y.; Sawa, R.; Homma, Y.; Igarashi, M.; Umezawa, K. J Antibiot (Tokyo) 2006, 59, 35-43.
53. Bhattacharjya, S.; Domadia, P. N.; Bhunia, A.; Malladi, S.; David, S. A. Biochemistry 2007, 46, 5864-5874.
54. Bhunia, A.; Chua, G. L.; Domadia, P. N.; Warshakoon, H.; Cromer, J. R.; David, S. A.; Bhattacharjya, S. Biochem Biophys Res Commun 2008, 369, 853-857.
55. David, S. A. J Mol Recognit 2001, 14, 370-387.
56. Nguyen, T. B.; Adisechan, A. K.; Suresh Kumar, E. V.; Balakrishna, R.; Kimbrell, M. R.; Miller, K. A.; Datta, A.; David, S. A. Bioorg Med Chem 2007, 15, 5694-5709.
57. Kraulis, P. J. J App Crystallogr 1991, 24, 946-950.

Table 1. Experimental and structural statistics for the family of 15 structures of *r*ALF-*Pm3*[a]

Distance restraints	
intraresidue (i-j = 0)	295
sequential (i-j = 1)	367
medium-range (i-j ≤ 5)	210
long-range (i-j >5)	221
total	1093
Dihedral-angle restraints	
ϕ	70
χ_1	10
χ_2	1
total	81
NOE violations	4.53 ± 1.73
Dihedral violations	0.067 ± 0.258
Mean rmsd from idealized covalent geometry	
bonds (Å)	0.003096 ± 0.000428
angles (°)	0.5288 ± 0.0086
impropers (°)	0.35566 ± 0.00979
Mean energies (Kcal.mol -1)	
E total	-514.09 ± 23.61
E bond	16.695 ± 0.714
E angle	126.34± 4.11
E improper	17.216 ± 0.947
E vdW	-311.21 ± 11.62
E noe	64.876 ± 6.837
E cdih	0.342 ± 0.223
Ramachandran (%)[b]	
Most favored	83.5
Additionally allowed	16.0
Generously allowed	0.2
Disallowed	0.2

Pairwise atomic rmsd (Å)

backbone atoms (8-101)	0.906 ± 0.29

---

[a] For these calculations, the XPLOR all-hydrogen force fields "topoallhdg" and "parallhdg all" were used. The final minimization of the 21 structures was made with force constants of 15 kcal mol^{-1} $Å^{-2}$ and 50 kcal mol^{-1} rad^{-2} for the NOE and dihedral angle potentials, respectively.
[b] Calculated with PROCHECK.

Table 2: Charged residues involved in the FhuA/lipid A interaction (pdb entry 1qfg) *(30*) and their counterpart for the *r*ALF-*Pm3* solution structure and the ALF-L cristallographic structure *(8*). Rmsd were calculated from backbone atoms of 20 residues belonging to the S1 to S4 strands. Values in parenthesis correspond to the 17 residues of the S2 to S4 strands. For ALF-T, corresponding residues were identified from the sequence alignment displayed in Figure 1.

Structure	Charged residues								rmsd (Å)
FhuA/LPS	E304	K306	K351	R382		R384	K439	K441	
*r*ALF-*Pm3*	E25	K26	K35	K50	K39*	R52	R52*	K50	1.38 (0.96)
ALF-L	-	-	H32/R34 K26*	K47	K36*	K49	R61*	-	1.52 (0.95)
ALF-T	-	-	H33	K48	-	K50	K50	K48	-

* means located on the neighbor strand

FIGURE LEGENDS

Fig. 1. Alignment of the ALF-*Pm3*, ALF-L and ALF-T sequences. The N-terminal tetrapeptide cloning sequences (EAYV for ALF-*Pm3* and EAEA for ALF-L) are displayed in italics. They were not taken into account for the alignment but for convenience included in the numbering. The numbering displayed is that of ALF-*Pm3*. Conserved residues (31.6%) in the three sequences are in bold. Helical and β-stranded structures of ALF-L *(8)* and of ALF-*Pm3* (this work) are highlighted in blue and pink, respectively. The C^{34}-C^{55} disulfide bond is displayed.

Fig. 2. Assignment of the ^{1}H-^{15}N-HSQC of the uniformly ^{15}N-labeled *r*ALF-*Pm3* (pH 6.9, 32°C). *W is for indole cross-peaks. Notice that the L^{30} cross-peak is out of the frame at 5.23 ppm.

Fig. 3. Structure of *r*ALF-*Pm3*. (Left) - Stereo view of the 10 best energies minimized conformers. The 8-101 heavy atoms of the backbone were used for the superimposition. The C^{34}-C^{55} disulfide bridge is displayed as dashed lines. (Right) - The structure prepared using MOLSCRIPT *(57)* shows the location of the 3 α-helices, the 4 β-strands and the C^{34}-C^{55} disulfide bond.

Fig. 4. Comparison of the *r*ALF-*Pm3* solution structure with that of the ALF-L crystal structure *(8)*. For the superimposition of the A^{4}-A^{98} of ALF-L backbone atoms with those of the 7-101 residues of *r*ALF-*Pm3* an rmsd value of 2.16 Å was measured. The graph shows that by using a five-residue sliding window significant differences appeared mainly for the loop between the H1 helix and the S1 strand. Without the H1 helix, an rmsd value of 1.19 Å was measured for the A^{29}-A^{98}/32-101 superimposition (70 residues). Helices and beta strands are indicated by blue and red bars, respectively. Black diamonds are for conserved residues.

Fig. 5. Surface plasmon resonance analysis. Sensorgrams of the interaction of *r*ALF-*Pm3* immobilized on CM5 sensor chip and lipid A derivatives at several concentrations in 10 mM HEPES, 150 mM NaCl buffer at pH 7.4 and 25 °C. (A), with *E. coli* LPS, (B) with lipid A, and (C) with the OM®-174 soluble analogue. Kinetic data of the interaction were calculated with the BIAevaluation 3.2 software using the bivalent analyte model. RU: resonance units. The chemical structures of the *E. coli* Lipid A and of OM®-174, the water soluble triacyl lipid A, are displayed above.

Fig. 6. Study of the *r*ALF-*Pm3* interaction with the *E. coli* LPS monitored by NMR (27°C, pH 6.70). Each ^{1}H-^{15}N NMR spectrum was recorded with 64 scans and 128 t1 points.
(A) The ^{1}H-^{15}N HSQC reference map of *r*ALF-*Pm3* was recorded with about 0.4 mg of protein (≈ 70 μM).
Upon the LPS addition (B: 0.04 mg, C: 0.14 mg, D: 0.24 mg), the HSQC cross-peaks progressively decreased in intensity to disappear with an excess of LPS. The spectrum with 1 mg of LPS is not shown. The *r*ALF-*Pm3*/LPS complex is aggregated and thus precipitated.

Fig. 7. Evolution of the LPS/*r*ALF-*Pm3* molar ratio upon the formation of the rALF-Pm3/LPS complex at room temperature. The initial concentration of *r*ALF-*Pm3* was 0.44 mg/ml. The concentration of the free ALF-*Pm3* in the supernatant was measured by UV after a 100.000 g ultracentrifugation for 30 min.

Fig. 8. Two 90° stereo views of the proposed ALF binding site delineated from the FhuA/LPS X-ray structure (pdb entry: 1qfg) *(30)*. (Left) Superimposition of the 7 to 10 beta strands of FhuA (green) with S1 to S4 beta strands of ALF-*Pm3* (orange). Positively and negatively charged side chains of FhuA interacting with LPS are displayed as blue and red sticks, respectively. The corresponding side chains of ALF-*Pm3* are displayed by thin lines and labeled (ALF-*Pm3* residue/FhuA residue). For clarity, the LPS and the three helices of ALF-*Pm3* were removed. The ALF-*Pm3* disulfide bond is in yellow. (Right) Comparison of the FhuA/LPS interface with the proposed lipid A-binding site for ALF-*Pm3*. The LPS is in purple with fatty acid chains and sugars in the upper and lower parts, respectively. The lipid A moiety is labeled. Phosphorus atoms are displayed as purple spheres. The proposed binding site would be in agreement with data indicating that the synthetic β-hairpin peptide of ALF-L binds to LPS *(15, 39-46*).

Figure 1

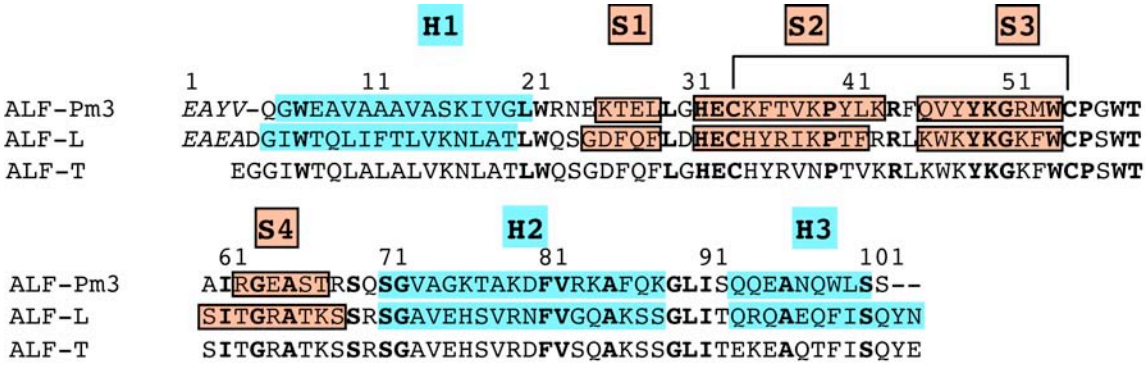

Figure 2

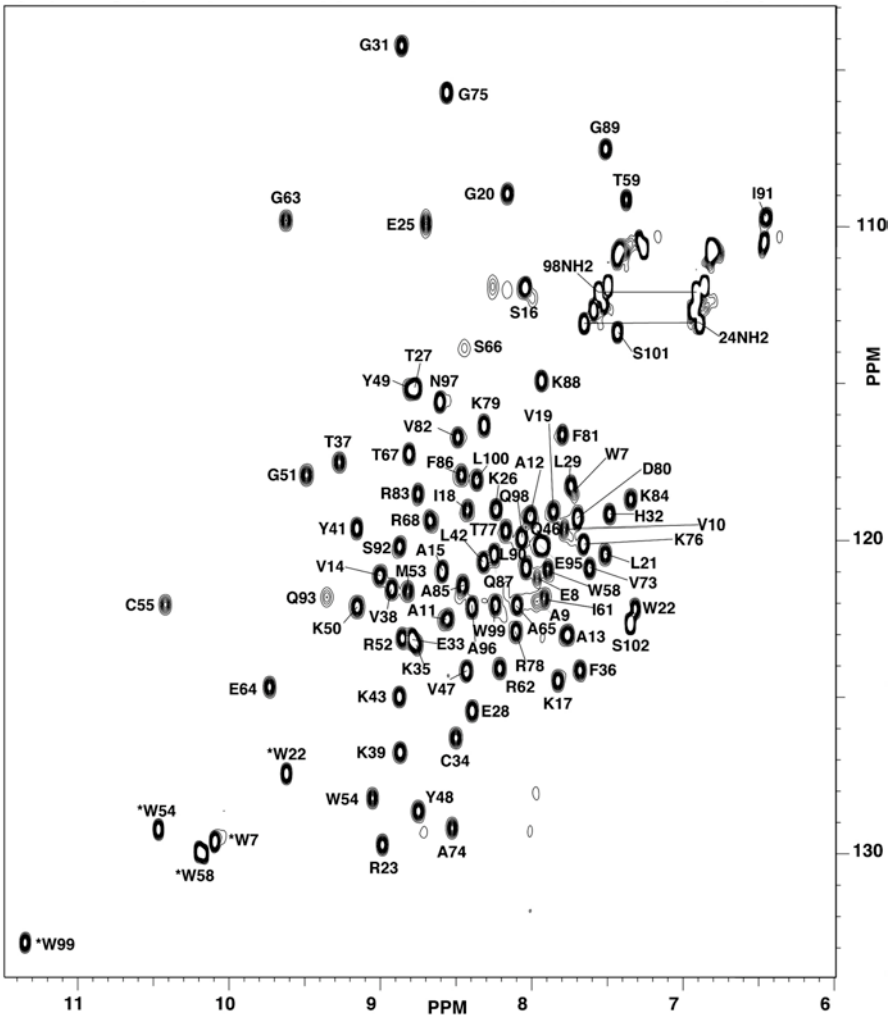

Figure 3

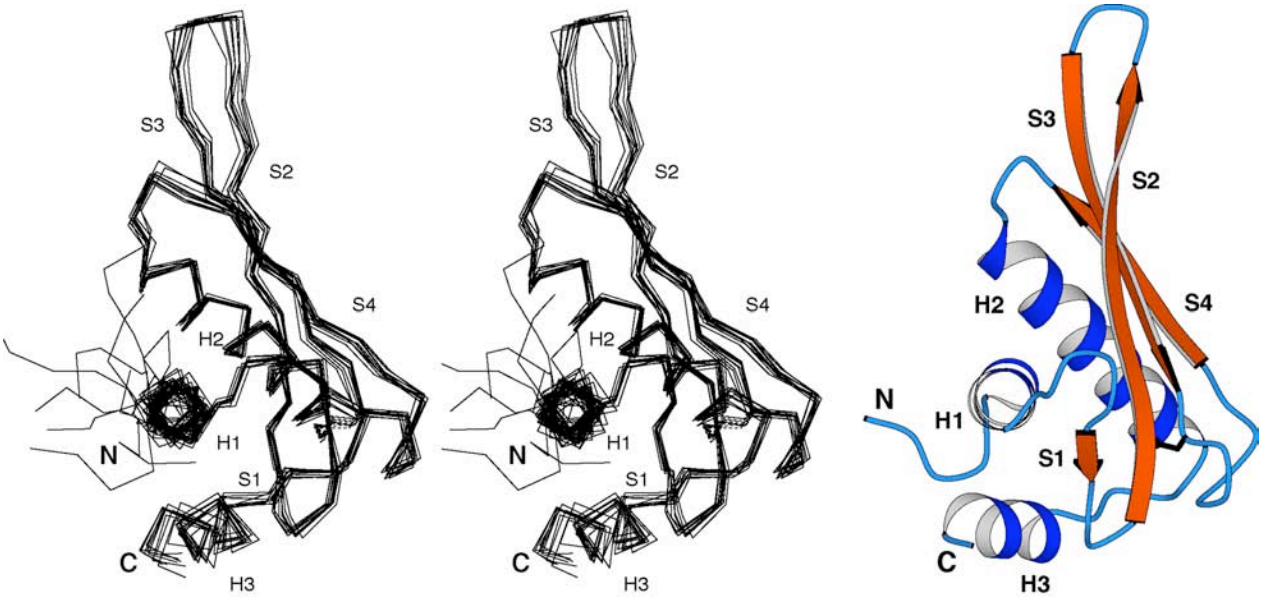

Figure 4

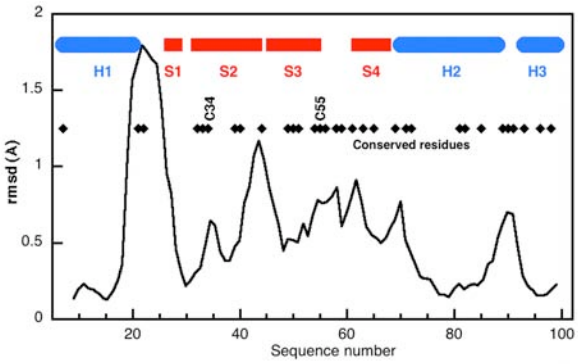

Figure 5

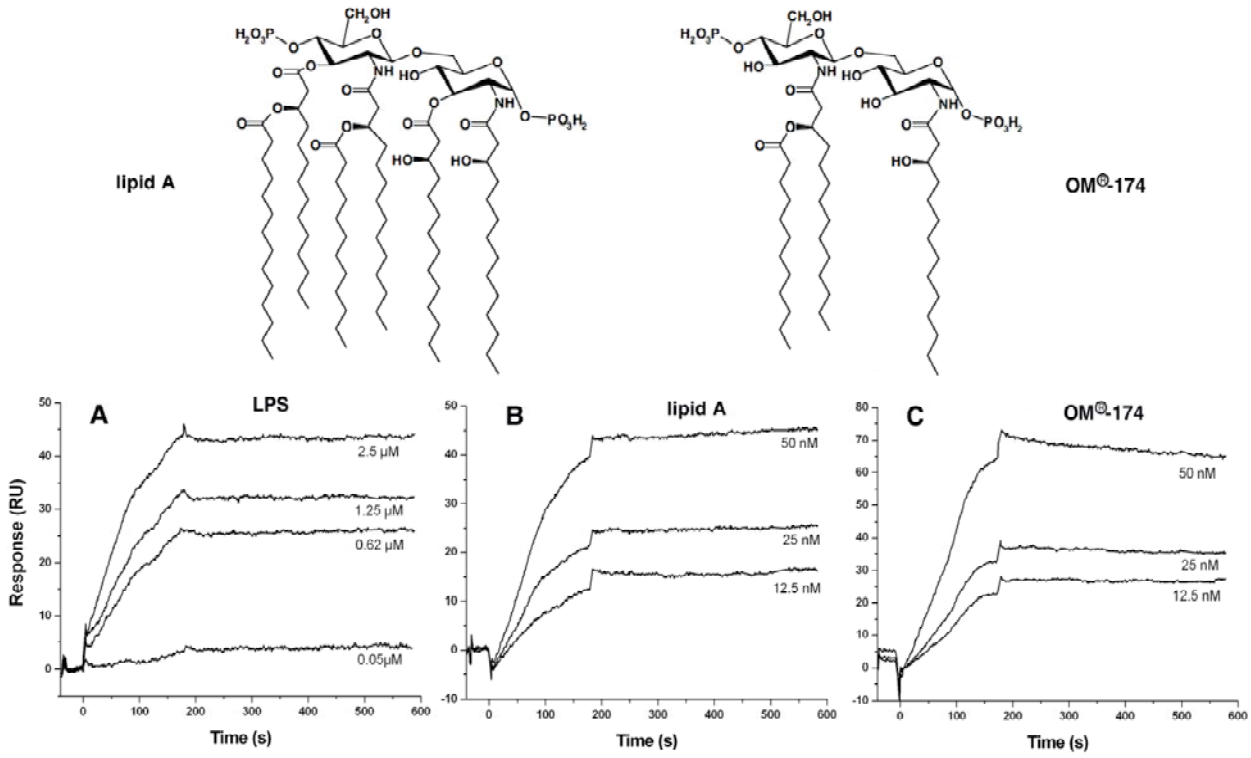
lipid A
OM®-174
A
LPS
2.5 µM
1.25 µM
0.62 µM
0.05µM
Response (RU)
Time (s)
B
lipid A
50 nM
25 nM
12.5 nM
Time (s)
C
OM®-174
50 nM
25 nM
12.5 nM
Time (s)

Figure 6

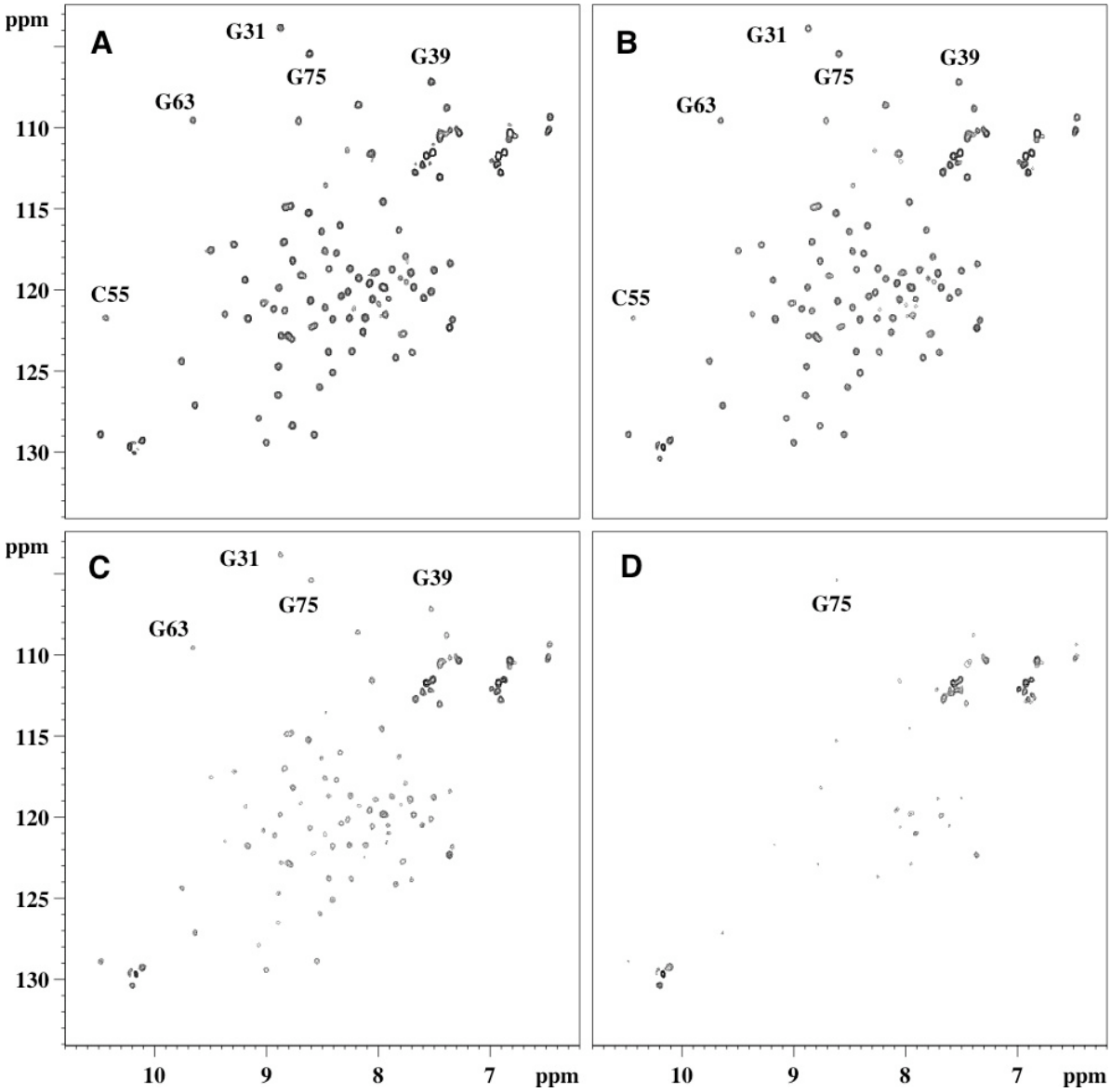

Figure 7

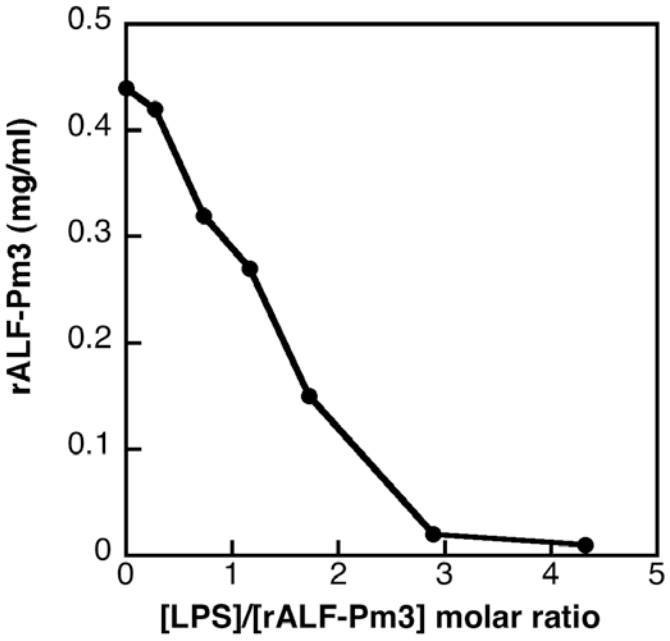

Figure 8

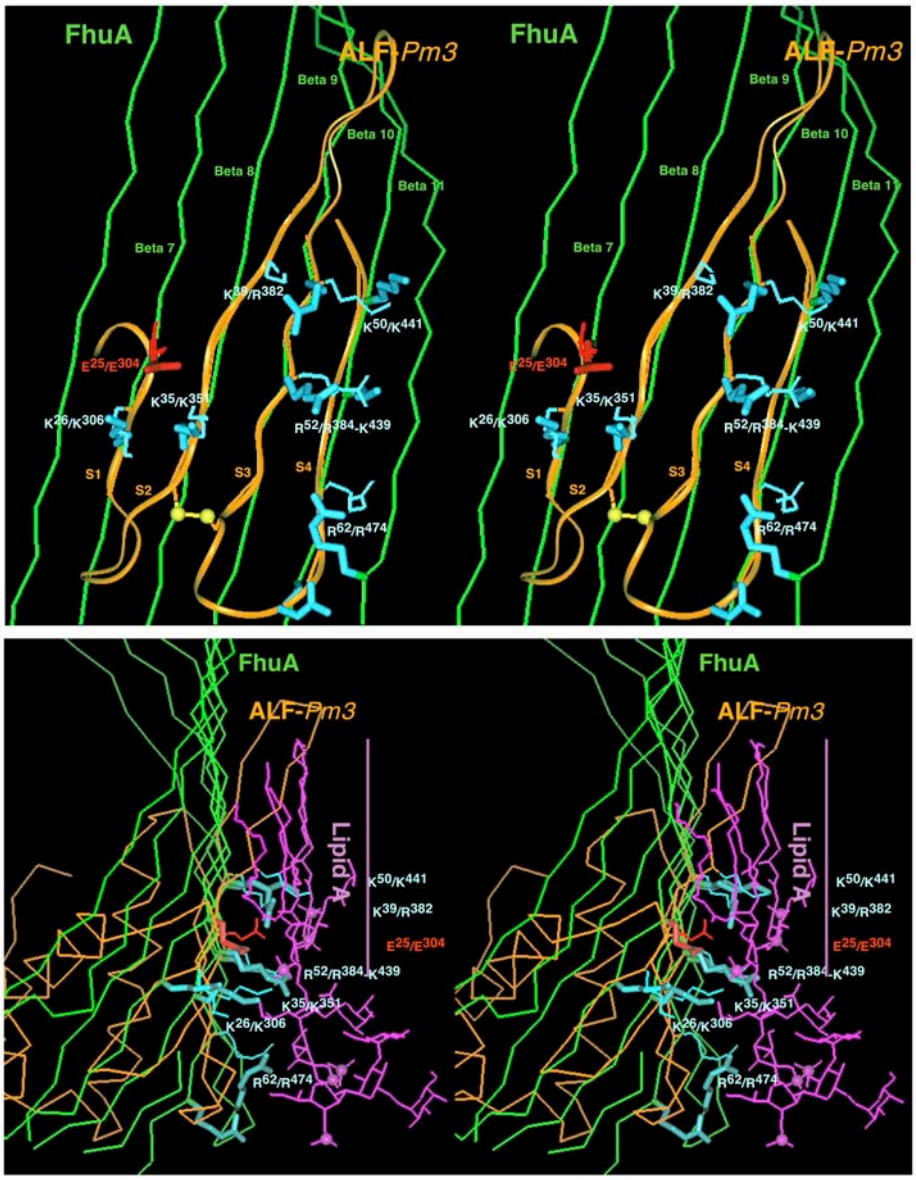
FhuA
ALF-Pm3
Beta 9
Beta 10
Beta 8
Beta 11
Beta 7
K39/R382
K50/K441
E25/E304
K35/K351
K26/K306
R52/R384-K439
S1
S2
S3
S4
R62/R474
FhuA
ALF-Pm3
Beta 9
Beta 10
Beta 8
Beta 11
Beta 7
K39/R382
K50/K441
E25/E304
K35/K351
K26/K306
R52/R384-K439
S1
S2
S3
S4
R62/R474
FhuA
ALF-Pm3
Lipid A
K50/K441
K39/R382
E25/E304
R52/R384-K439
K35/K351
K26/K306
R62/R474
FhuA
ALF-Pm3
Lipid A
K50/K441
K39/R382
E25/E304
R52/R384-K439
K35/K351
K26/K306
R62/R474

Supplementary material

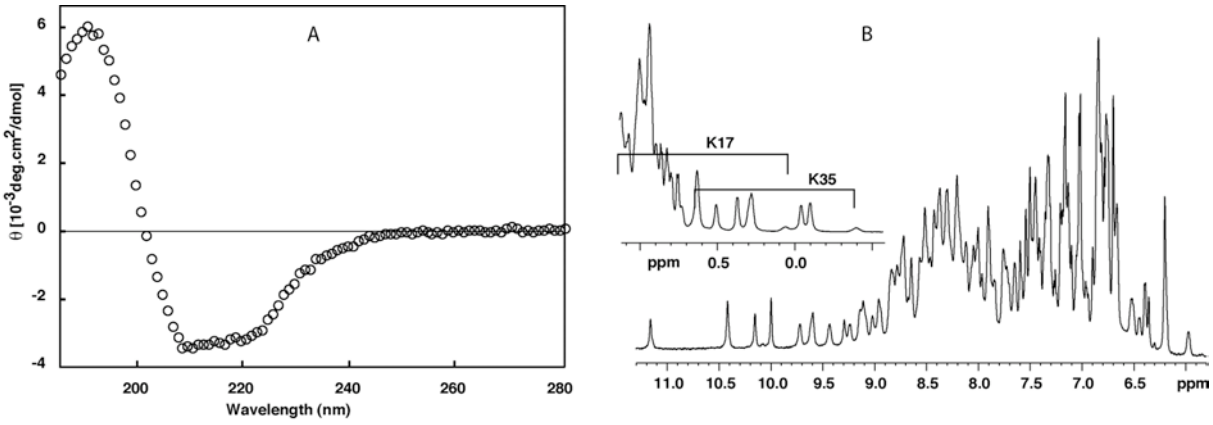

Figure 1S. CD and ^{1}H-NMR spectrum of the purified folded *r*ALF-*Pm3*.

(Left) The CD spectrum of *r*ALF-*Pm3* was recorded in water (20 °C, pH 6.9). The α-helix and β-sheet structures account for around 23-28 and 23-27%, respectively. (Right) Two selected parts of the ^{1}H-NMR spectrum: the low-field area (11.3 - 5.8 ppm) with the indole, amide and aromatic signals and the up-field area (1.1 - -0.6 ppm) with methyl signals show the spreading of resonances which is indicative of a well-defined 3D structure for *r*ALF-*Pm3* (32°C, pH 6.9). Notice the unusual up-field shifts of the K^{35} ββ ' and K^{17} γγ 'proton resonances.

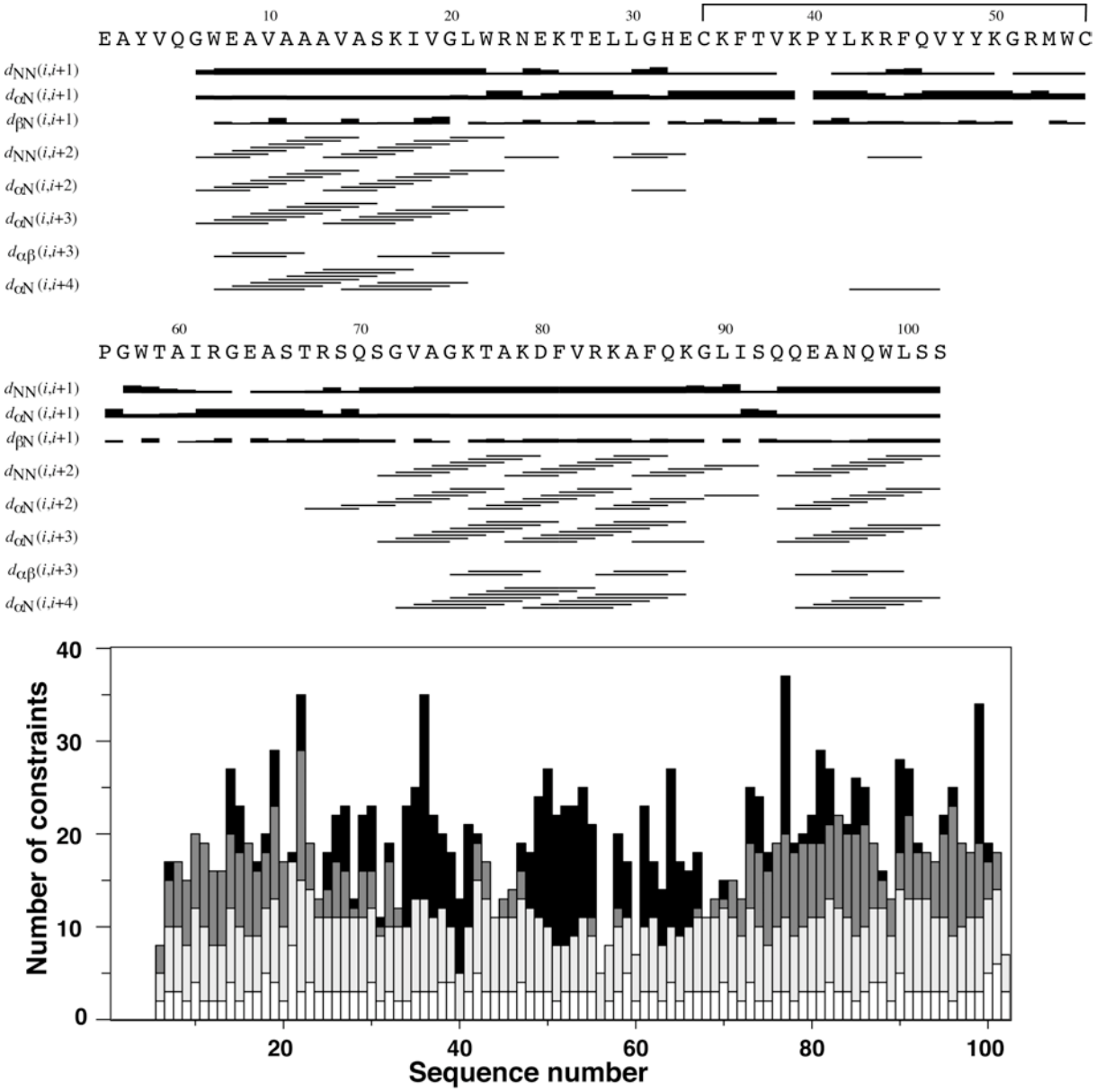

Fig. 2S. Summary and distribution of NOEs for *r*ALF-*Pm3*.

(Upper part) Summary of the sequential, medium-range, and long range NOEs. The relative intensity of NOEs is represented by the thickness of the bars. The C^{34}-C^{55} disulfide bond is displayed on the sequence.

(Lower part) Distribution of intra-residual (white), sequential (light gray), medium range (dark gray), and long range (black) constraints all along the sequence.